A comprehensive assessment of endogenous bubbles properties in fluidized bed reactors via X-ray imaging

Stefano Iannello, Domenico Macrì, Massimiliano Materazzi*

Department of Chemical Engineering, University College London, London WC1E 7JE, UK

* Corresponding author.

E-mail address: massimiliano.materazzi.09@ucl.ac.uk

Postal address: Roberts Engineering Building, University College London, Torrington Place, London WC1E 7JE

Abstract

Properties of endogenous bubbles released during the devolatilization of a single biomass particle under inert conditions have been investigated by means of advanced X-ray imaging techniques. Distribution of void fraction showed that endogenous bubbles structure resembles that of classic bubbles observed in fluidized bed reactors, constituted by a cloud, wake and a central void region. A value of about 0.25 for the wake fraction has been obtained from experiments, which is in agreement with literature data for Geldart B particles. Volume of cloud region as a function of relative bubble velocity was generally well-described by the theoretical models of Davidson and Murray, showing effective recirculation of volatile matter around the bubble. Moreover, lack of mixing between bubbles and emulsion phase, as predicted by the Davidson's theory for classic bubbles, confirmed the bypass phenomenon observed for endogenous bubbles in previous studies. Owing to the non-invasive nature of the X-ray technique employed, it was possible to estimate the main features of endogenous bubbles with high accuracy. Knowledge provided in this work can be easily implemented to improve modelling of fluidized bed reactors applied to advanced thermochemical conversions, such as gasification and pyrolysis, of biomass and waste materials.

Keywords

Devolatilization; Fluidized bed; Biomass conversion; Endogenous bubbles; X-ray imaging

1. Introduction

Bubbling fluidized bed reactors represent one of the most promising technologies for the production of renewable energy and valuable products from biomass and waste materials. Their excellent operation flexibility, mass and heat transfer features make fluidized bed reactors particularly suitable for processing highly heterogeneous solid feedstocks under a broad spectrum of operational conditions, from pure oxidizing to completely inert reaction environment. In the last few decades, there has been a renewed interest in using fluidized bed reactors for advanced thermochemical conversions, such as gasification and pyrolysis, where the solid feedstock is converted into valuable gaseous, liquid and solid products, in order to promote the green energy transition [1–6]. Nevertheless, bubbling fluidized bed reactors remain the main focus of current research, owing to unsolved issues related to poor mixing of both solid and gas phases [7–12]. In this context, there are two main phenomena occurring during the conversion of a solid feedstock, i.e., segregation and self-segregation. The former phenomenon is related to the reacting feedstock itself, which tends to stratify at the surface of the bed, due to its relatively lower density compared to that of typical bed materials [13–16], such as sand and alumina-silicate catalysts. This results in poor contact with bed inventory and subsequent reduced heat transfer, which is essential for high product yields and quality [17,18]. On the other hand, self-segregation is related to the evolution of the feedstock's volatile content during the first step of most thermochemical conversion, i.e., the devolatilization stage. At sufficiently high temperatures, a solid fuel releases volatiles into the bed in form of bubbles, called endogenous bubbles [13,19]. These are different from exogenous bubbles, which form when the superficial velocity of the gas used to fluidize the bed (e.g., air, nitrogen, CO_2, steam, or a combination of these) exceeds the minimum fluidization velocity of the bed material. Both segregation and self-segregation are closely connected to one another, since endogenous bubbles further enhance the rising velocity of the feedstock particles up to the bed surface, exerting a drag effect or lift force [13–15,20,21]. Several literature studies have shown that a lack of mixing occurs between bed emulsion phase and endogenous bubbles released, which ultimately erupt at the surface of the bed and release the volatile content into the freeboard of the reactor in a discontinuous pattern [13–16,22]. This observation is in contrast with the assumption of full mixing and instantaneous devolatilization, usually used to model thermochemical conversions of solid feedstocks in fluidized beds [23–31]. In addition, this implies the absence of a reacting solid phase, which migrate within the bed and continuously releases volatiles during operation, affecting the hydrodynamic of the entire reactor.

Exogenous bubbles have been extensively investigated and their mechanism of formation well-described through mathematical models [32–37]. Different diagnostic techniques have been used in the past to investigate the movement of an isolated object within a fluidized bed at cold conditions, including PIV (Particle Image Velocimetry), Lagrangian sensors, MPT (Magnetic Particle Tracking) and RPT (Radioactive Particle Tracking) [7,38,47–49,39–46]. However, none of these methods provide any information on the gas released by fuel particles reacting within the bed, and its interaction with the other gas phases at high operating temperatures. Among the available techniques, X-ray imaging is the only one, at present, to have the potential of carrying out this type of investigation, due to the possibility of direct visualization of dynamic phenomena occurring within the reactor, e.g., evolution of volatile matter from a solid feedstock, with high spatial and time resolutions [13,22]. The visualization is made possible thanks to the difference in density, hence attenuation of the X-ray beam, between gas and solid phases, without interfering with them. X-ray studies demonstrated that three-dimensional exogenous bubbles in a fluidized bed are remarkably spherical, apart from the particle wake filling the bottom [34]. Rowe and Partridge quantified the fraction of the bubble filled by the wake from numerous X-ray measurements and for different bed materials at ambient temperature [50]. Yates et al. investigated the void distribution in exogenous bubbles via X-ray imaging and observed the presence of an expanded shell of gas and particles surrounding the bubbles, where the porosity is much lower than that observed for the emulsion phase. They also observed a similar behaviour for the wake region of the bubbles [51]. X-ray imaging techniques have been also successfully applied in more recent studies regarding horizontal jet penetration in gas fluidized beds [52,53].

However, the present literature lacks knowledge regarding the evolution of endogenous bubbles released during devolatilization at typical conditions of industrial thermochemical processes. The great amount of gas released by a highly volatile feedstock can have an impact on the mixing of the bed solids. This results in an alteration of heat transfer properties of the bed itself, which must be taken into account to improve existing modelling techniques [23]. Furthermore, the interaction between volatile matter and fluidization medium may significantly be affected by the eruption of endogenous bubbles at the bed surface (i.e., splashing zone), where the mass transfer and chemical reactions mainly occur [30,54]. As a consequence, the whole concentration profile of the released gas species along the rest of the reactor (freeboard zone) is also affected. Characterization of the volatiles distribution within a fluidized bed is then crucial for development and design of high-performance operations. The present work aims at providing a deeper understanding of endogenous bubbles properties, with emphasis on their void distribution and structure obtained by means of X-ray imaging techniques.

2. Material and methods

2.1 Experimental unit

The experimental apparatus consists of a 146 mm ID × 1000 mm high Inconel tube fitted with a stainless-steel distributor plate and is operated at atmospheric pressure and temperature of 730 °C, in order to provide devolatilization of the biomass particle injected. The vessel was filled with a Geldart group B quartz sand (particle density 2650 kg/m^3 and average particle size 250 μm) up to a fixed bed height of 20 cm at ambient temperature. The reactor is electrically heated and insulated with multiple layers of rockwool to maintain the high bed temperature and reduce heat losses as much as possible. Nitrogen was used as fluidizing medium and the bed was operated at minimum fluidization (U_{mf} = 1.74 cm/s at 730 °C) for all the experiments to enable observation of volatiles without possibilities of confusion arising from exogenous bubbles. Figure 1 shows the experimental apparatus used.

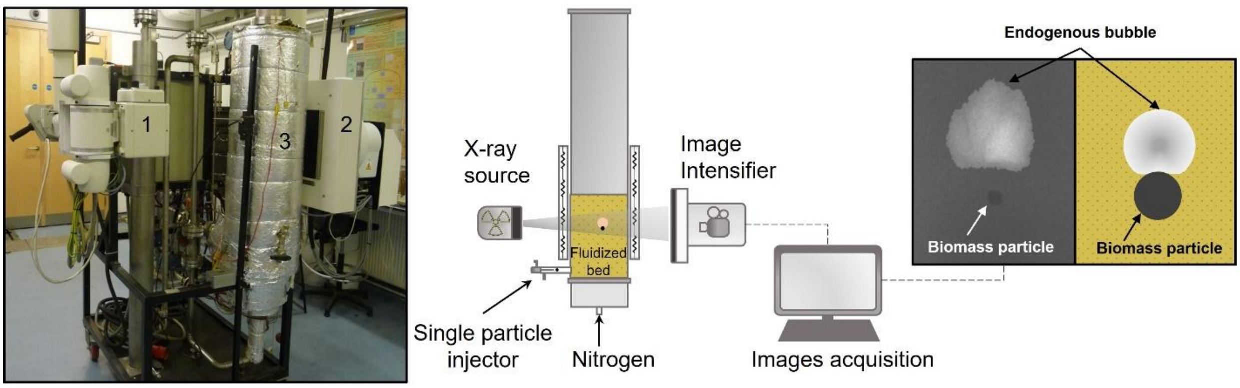

Figure 1: Experimental apparatus. 1: X-ray source, 2: Image intensifier, 3: Fluidized bed reactor.

The fluidized bed reactor is placed in between X-ray source and image intensifier, in order to visualize the endogenous bubbles released by the single biomass particle. A 12-mm beech wood spherical particle was injected from the bottom of the fluidized bed by means of a single fuel particle injector located at 2.5 cm above the distributor plate. Typical physical and chemical properties of the materials investigated are listed in Table 1.

Table 1: Typical physical and chemical properties of beech wood (BW).

	BW		
Ref.	[55]	[56]	[57]
Ultimate analysis, (wt%)	db	daf	db
C	48.1	49.2	49.1
H	5.9	6.0	5.7
O	45.4	44.1	44.5
N	0.2	0.5	0.15
S	-	0.02	0.045
Proximate analysis, (wt%)	wb	db	db
Volatiles	74.8	85.3	84.3
Fixed carbon	15.7	14.3	15.2
Ash	0.7	0.4	0.5
Moisture	8.8	0	8.7^{ar}
Heating value db, [MJ/kg]	15.0	-	-

ar: as received, daf: dry ash free, db: dry basis, wb: wet basis

Once the particle reaches the surface of the bed, it continues releasing its volatile content into the freeboard. Therefore, the properties of endogenous bubbles were assessed via X-ray imaging during the residence time of the particle within the bed.

2.2 X-ray imaging technique and analysis

The X-ray methodology used relies on a series of non-invasive techniques, capable to provide frame-by-frame imaging with extremely high time and spatial resolution of 36 frames per second and about 1.6 mm/pixel, respectively. The conversion factor from pixel to SI units has been calculated by placing a square lead marker of known size (1 × 1 cm) on the external surface of the reactor. Different algorithms for image analysis were developed and implemented in MATLAB® [22,58], in order to enhance the quality of the images and perform any quantitative analysis. The image post-processing procedure must take into account the intrinsic curvature of the image intensifier and diverging conical shape of the X-ray beam, also known as pincushion distortion. This undesirable effect was reduced by decreasing the distance between the reactor and image intensifier (optimal value of 26 cm) and increasing the distance between X-ray source and image intensifier (optimal value of 99 cm). The quality of the images collected was improved by applying contrast and filtering functions. Although the X-ray facility allows to visualize the entire bed, a smaller region of interest has been chosen to post-process the images, in order to focus the analysis on the endogenous bubbles only. Figure 2 shows an example of image processing performed on a single endogenous bubble with different levels of detail.

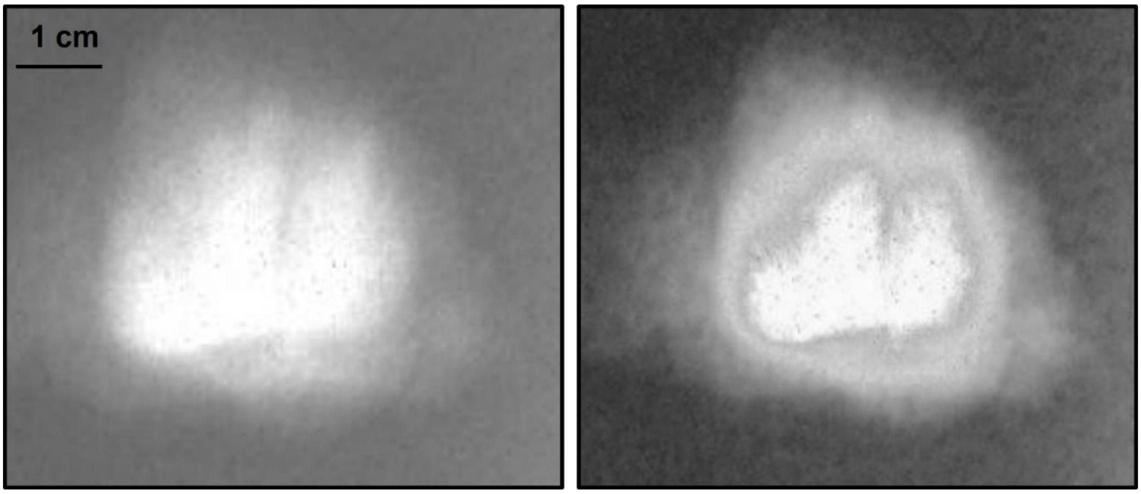

Figure 2: Two-dimensional X-ray visualization of a three-dimensional endogenous bubble. Raw image (left) and post-processed image (right) after application of contrast and filtering algorithms.

Measurements of bubbles size, structure, velocity and frequency of formation have been carried out on each chosen endogenous bubble during the in-bed devolatilization of the biomass particle. The images were collected fixing the height of the X-ray source at 17 cm from the distributor plate. The image intensifier was then synchronized to the source at same height to provide visualization and images acquisition. Generally, a gas bubble increases in size during its rise, therefore the height of 17 cm was chosen to ensure that the bubble was well-developed, but still far from its eruption at the bed surface, to provide high quality visualization and quantitative measurements. Results obtained are shown and discussed in the next section.

The high difference in attenuation of X-ray beams between solid and gas phases allows to visualize the volatiles bubbles and distinguish them from the bed material very clearly. Investigation of bubbles void fraction is based on the Beer-Lambert equation [51,59–61]:

$$I = I_0 e^{-\mu c L} \quad (1)$$

where I is the transmitted intensity, I_0 the incident intensity, μ the attenuation coefficient of the particulate material, c its concentration and L the path length of the X-ray beam. Eq. 1 can be expanded to its linear form and the second and higher order terms in the exponential may be neglected, as follows:

$$I = I_0 - I_0(\mu c L) \quad (2)$$

Such an approximation was justified by Yates et al. to be accurate with a linear correlation coefficient of 0.997 [51,61,62]. Since the attenuation of X-rays of volatile matter is negligible, the concentration, c, can be expressed in terms of the solids fraction of the fluidized bed through which the beam passes. Considering ε as the average void fraction of the bed material along the path length, Eq. 2 can be written as:

$$I = I_0 - I_0\mu(1-\varepsilon)L \quad (3)$$

Once a reference image of the packed bed with known void fraction is acquired, the value of ε corresponding to each path length can be obtained [62]. Eq. 3 applied to the packed bed image provides the coefficient μL for the specific particulate material, which can then be used to obtain the void fraction for the spatial grayscale intensity distribution associated with each frame.

Physical structure of endogenous bubbles has been assessed on each postprocessed X-ray image, using ImageJ software.

3. Results and discussion

3.1 Void fraction distribution in endogenous bubbles

Figure 3 shows one of the X-ray frames along with the distribution of void fraction selected for the discussion.

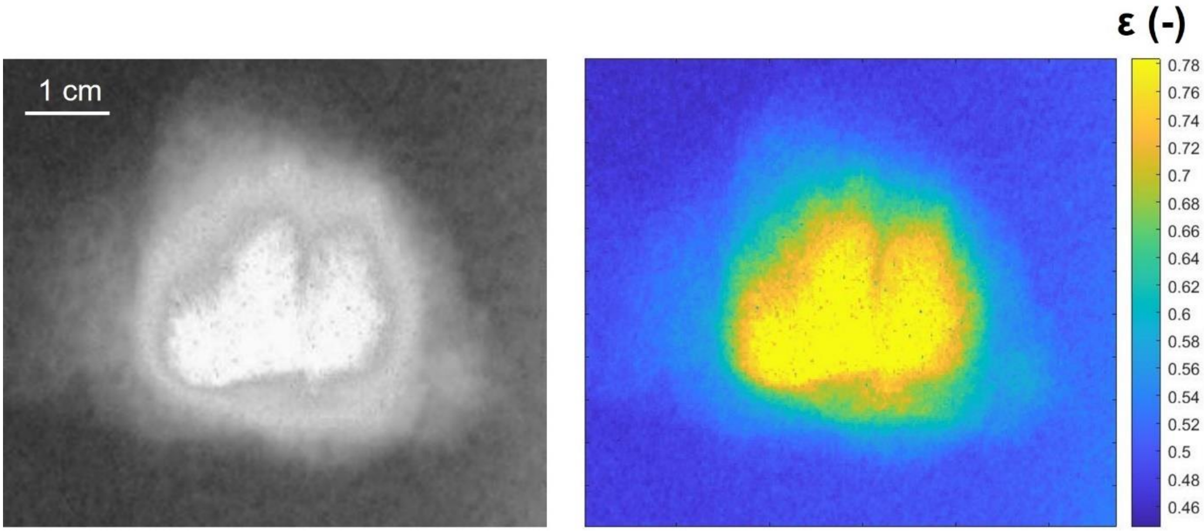

Figure 3: Void fraction distribution of an endogenous bubble. Left: Post-processed frame of an endogenous bubble. Right: two-dimensional void fraction distribution ε for the same endogenous bubble.

It can be observed that low values of void fraction of about 0.47 correspond to the emulsion phase. In the proximity of the endogenous bubble, the concentration of bed solids decreases, and it is possible to distinguish three main regions according to the measured values of void fraction. This observation shows that the structure of an endogenous bubble is similar to that of an exogenous bubble, which has been extensively investigated, as reported in several research studies present in literature [32,35–37,63]. In particular, Davidson proposed a model where the bubble generally consists of a cloud, wake and central void phase, which has been used by many authors to describe the fluid dynamics of fluidized beds [32,38,39,43,44,64]. Moreover, several researchers used the Davidson's assumption to model fluidized bed reactors applied to thermochemical conversions, showing good predictive capabilities [23,30,45,65]. Results obtained in this work show that an endogenous bubble has a similar structure to the Davidson's bubble, therefore the three observed regions of void fraction can follow the same definitions.

Figure 4 shows intensity distribution for the same endogenous bubble reported in Figure 3. Intensity of the X-ray beam passing through the emulsion phase and endogenous bubble is represented by values of grey scale, where zero and 255 correspond to black and white, respectively. The values of intensity reported in the graphs have been obtained along either a horizontal (Figure 4-a) or a vertical line (Figure 4-b) passing through the centre of the bubble.

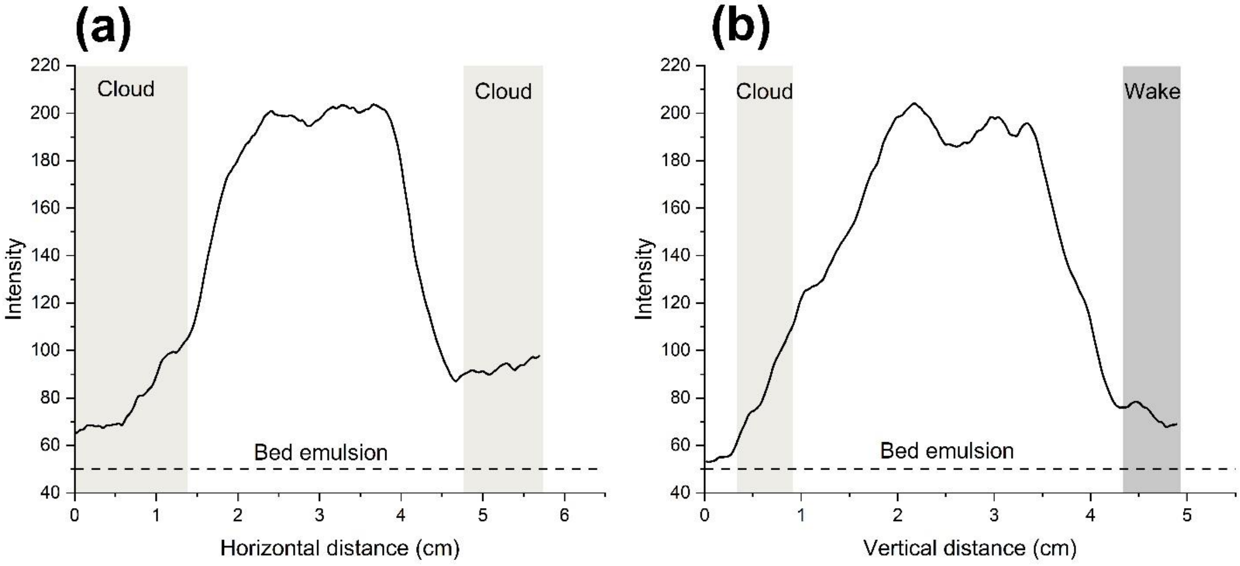

Figure 4: Intensity across the equator (a) and meridian (b) of an endogenous bubble.

In the present case, the intensity starts from a minimum value of about 50 representing the emulsion phase and it increases as the X-ray beam enters the expanded regions of cloud and wake until the centre of the bubble, where the concentration of bed particles reaches its minimum value. As can be seen from the graphs, the intensity distribution along both the horizontal and vertical direction follows a similar trend, showing symmetry of the bubble released. It can be noticed that the cloud region has generally a larger volume than the wake region, as demonstrated by the hydrodynamic theories [32]. Further details are reported in the next section.

Figure 5 shows the distribution of void fraction for cloud and wake regions of the endogenous bubble. Values of ε are shown along either a horizontal or a vertical line passing through the centre of the bubble.

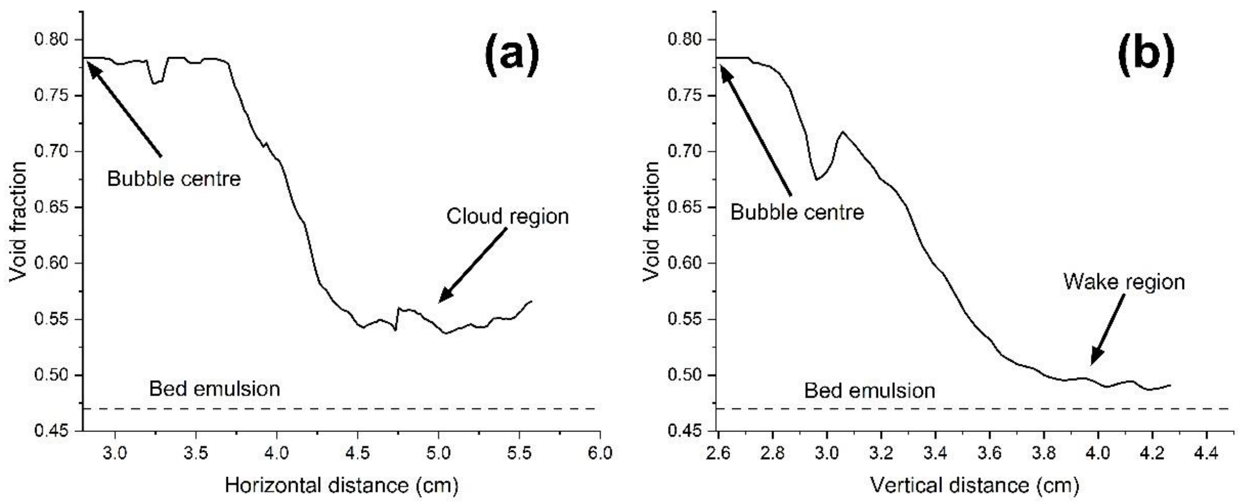

Figure 5: Void fraction across the equator (a) and meridian (b) of an endogenous bubble.

Since the void fraction is related to the intensity of the X-ray beam through the Beer-Lambert equation (Eq. 3), epsilon follows the same behaviour of *I*, discussed in the previous section. In fact, results showed in Figure 5 have been obtained using values of intensity reported in Figure 4. The void fraction of the expanded bed at minimum fluidization is 0.47, as showed in the graphs, and it reaches its maximum of 0.78, which corresponds to the highest concentration of volatile matter at the centre of the bubble. Similar trends can be observed for both Figure 5-a and Figure 5-b. However, the void fraction in the wake phase (Figure 5-b) along the vertical axis is noticeably lower than that in the cloud region, indicating a relatively higher concentration of solids travelling behind the rising bubble. The wake zone in endogenous bubbles may be responsible for the establishment of a drag effect exerted on the reacting fuel particle, which existence has been observed by other researchers [13–16,21]. According to Solimene et al., a fully-formed endogenous bubble transfers momentum to the gas-emitting particle [21]. X-ray measurements conducted by Rowe et al. showed that the upward movement of solid particles is associated to that of the wake of rising bubbles [37]. From these observations, it can be then assumed that the induced endogenous bubbles lift effect is due to the presence of a wake phase.

3.2 Assessment of bubbles structure

3.2.1 Wake region

From the images collected it was also possible to measure the volumes of each zone of the endogenous bubbles. Figure 6 shows an endogenous bubble and the method used to measure the volume of its wake region.

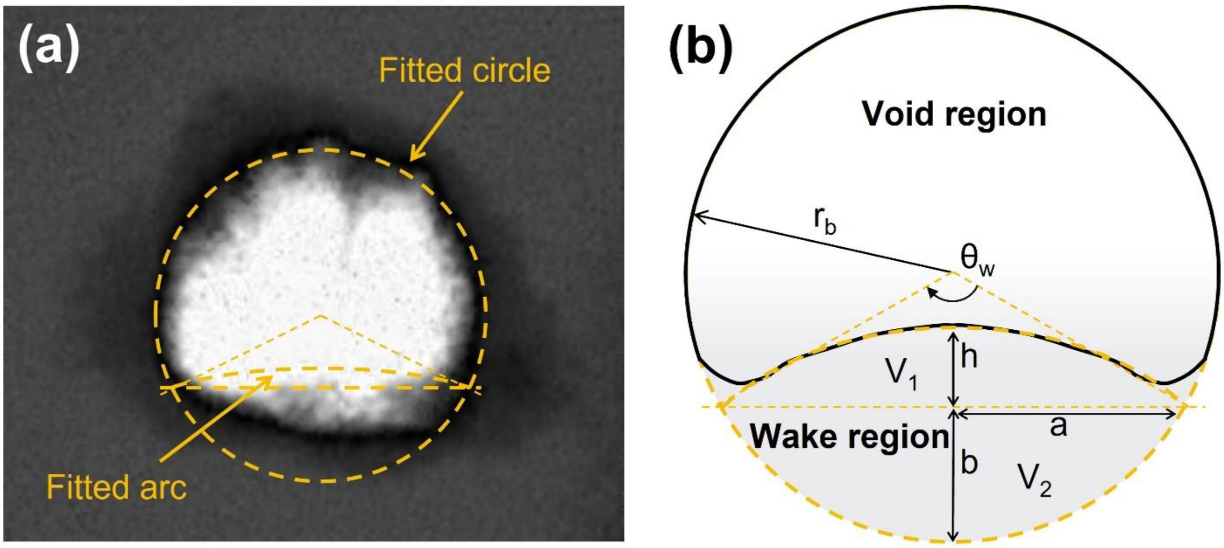

Figure 6: X-ray visualization of an endogenous bubble (a) and measurement criterion of its wake region (b).

The volume of wake can be considered as the sum of two spherical caps with volumes V_1 and V_2, having the same radius a, and height h and b, respectively (Figure 6-b). These volumes are given by the following equations:

$$V_1 = \frac{\pi}{6} h(3a^2 + h^2) \tag{4}$$

$$V_2 = \frac{\pi}{6} b(3a^2 + b^2) \tag{5}$$

The second volume can be also expressed in terms of the bubble radius and wake angle as:

$$V_2 = \frac{\pi}{3} r_b^3 \left(2 - 3\sin\frac{\theta_w}{2} + \sin^3\frac{\theta_w}{2}\right) \tag{6}$$

Each bubble was assumed to be spherical and the equivalent circle in each X-ray frame to represent the cross-sectional area of the bubble itself. After measurement of all the physical parameters r_b, h, and θ_w, it was possible to calculate the volume of wake region as:

$$V_w = \frac{\pi}{6} h(3a^2 + h^2) + \frac{\pi}{3} r_b^3 \left(2 - 3\sin\frac{\theta_w}{2} + \sin^3\frac{\theta_w}{2}\right) \tag{7}$$

The fraction of the endogenous bubble occupied by the wake is given by the following equation:

$$f_w = \frac{3\,V_w}{4\,\pi\,r_b^3} \tag{8}$$

Measurements of the parameters r_b, a, b, h and θ_w were conducted as explained in Figure 6-b, using ImageJ software on each postprocessed X-ray frame.

Table 2 shows the results obtained from X-ray measurements of 18 different endogenous bubbles at the same height within the bed of 17 cm from the distributor plate, where the bubbles were clearly visible and developed.

Table 2: Results obtained from X-ray measurements of the wake phase.

Bubble (#)	**r_b (cm)**	**θ_w (deg)**	**f_w**
1	1.33	130	0.240
2	1.36	129	0.264
3	1.57	114	0.267
4	1.38	118	0.217
5	1.64	116	0.194
6	0.889	104	0.289
7	0.931	116	0.221
8	1.13	129	0.218
9	1.07	115	0.217
10	1.01	116	0.405
11	1.37	129	0.170
12	0.909	116	0.266
13	1.30	127	0.273
14	1.51	105	0.165
15	1.27	127	0.244
16	1.09	114	0.366
17	1.19	129	0.271
18	0.919	118	0.269

The value of wake fraction f_w measured in this study is 0.253 ± 0.0603 and is in line with values for exogenous bubbles found in literature. Rowe and Partridge measured f_w for different types of bed material using X-ray imaging techniques and obtained values between 0.21 and 0.26 for natural sand [50].

3.2.2 Cloud region

Figure 7 shows the shape of the cloud region of endogenous bubbles assumed for the calculations. The fitted circle was chosen according to the values of intensity/void fraction in each frame. The area of the images where the intensity (or void fraction) reaches an almost constant value, which lower than the one measured for the void region and higher than that of the emulsion phase (Figure 4 and 5), has been assumed to be occupied by the bubble's cloud.

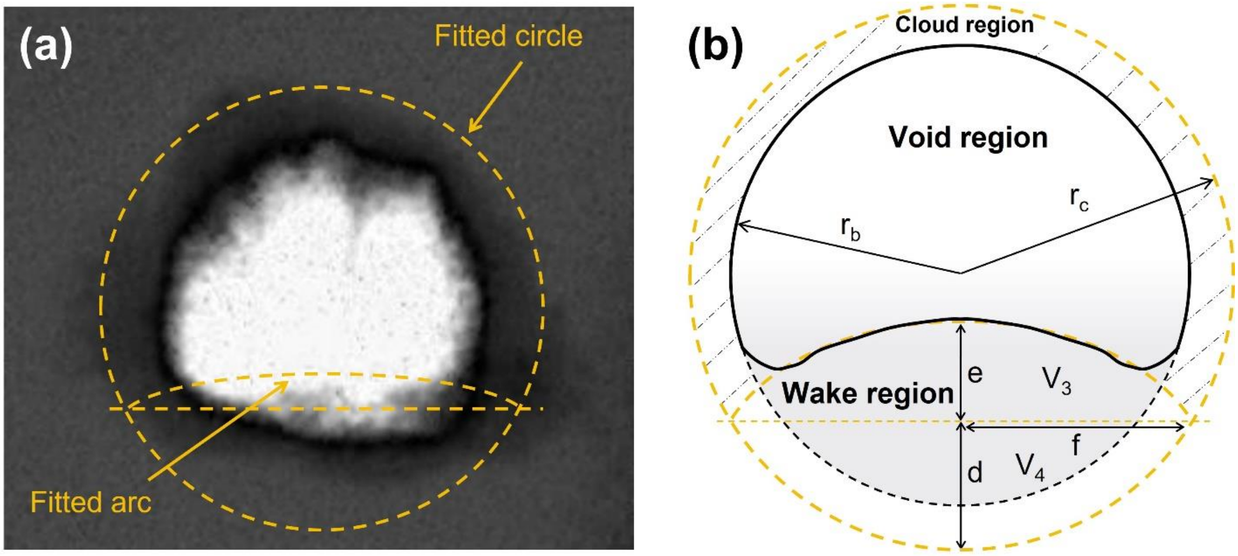

Figure 7: X-ray visualization of an endogenous bubble (a) and measurement criterion of its cloud region (b).

According to Figure 7-b, the volume of the actual cloud region (V_c) has been calculated by subtracting two spherical caps with volumes V_3 and V_4 from a fitted sphere (V_{fit}) surrounding the bubble and its cloud. The two volumes represented in Figure 7 can be calculated following the same procedure used for V_1 and V_2 discussed in the previous section, as follows:

$$V_3 = \frac{\pi}{6} e(3f^2 + e^2) \tag{9}$$

$$V_4 = \frac{\pi}{6} d(3f^2 + d^2) \tag{10}$$

For ease of measurements, the cloud region has been assumed to have the same boundary (or same fitted arc) of the wake phase. The volume of the cloud region can be calculated as follows:

$$V_c = V_{fit} - \frac{\pi}{6} e(3f^2 + e^2) - \frac{\pi}{6} d(3f^2 + d^2) \tag{11}$$

Eq. 11 can be written in terms of the radius of the cloud region, as follows:

$$V_c = \frac{4\,\pi}{3} r_c^3 - \frac{\pi}{6} e(3f^2 + e^2) - \frac{\pi}{3} d^2(3r_c - d) \tag{12}$$

where r_c is the radius of the cloud. Measurements of the bubble's physical parameters in Figure 7 were conducted in ImageJ software, as for the wake region assessment explained in previous section.

It is interesting to compare the experimental cloud size with the calculated values from the most well-known theoretical models for three-dimensional bubbles by Davidson and Murray.

Davidson's equation:

$$\frac{r_c}{r_b} = \left(\frac{\alpha + 2}{\alpha - 1}\right)^{1/3} \tag{13}$$

Murray's equation:

$$(\alpha - 1)\left(\frac{r_c}{r_b}\right)^4 - \alpha \frac{r_c}{r_b} - 4\cos\omega = 0 \tag{14}$$

where $\alpha = \varepsilon_{mf}\, U_{br}/U_{mf}$ is the relative bubble velocity. In this context, ε_{mf} represents the void fraction of the bed at minimum fluidization condition. The cloud forms as the emulsion gas passes through the bubble from bottom to top. According to Davidson, when a bubble travels faster than the interstitial fluidizing medium, the gas starts recirculating around the bubble after leaving its upper part, hence generating the cloud region [32]. In the present case, however, the fuel particle releases continuously volatile matter below each generated endogenous bubble. A part of this gas percolates through the emulsion phase and does not form any bubble. It is then possible to make the following assumptions to describe the mechanism of cloud formation:

- Only the fraction of volatile matter that percolates through the emulsion behind a rising endogenous bubble is responsible for the generation of its cloud.
- The interstitial velocity of volatile matter in the emulsion phase is given by the kinetic of devolatilization of the fuel particle.

The first assumption is in line with previous research studies, where several authors observed that the gas in the dense bed does not interact with the endogenous bubbles [16,22].

The volume of the bubble measured via X-ray imaging depends on the flow rate of volatile matter released during the devolatilization and can be calculated as follows:

$$V_b = \gamma \frac{Q}{n_b} \tag{15}$$

where n_b is the frequency of bubbles formation obtained from experiment. The measured value from X-ray images is 7.53 ± 0.72 s^{-1}, which is very close to the one obtained by Kunii and Levenspiel of about 7 s^{-1} for the formation of bubbles from an orifice [32]. The parameter γ depends on the temperature at which the devolatilization occurs [22]. However, Eq. 15 can be also written in terms of visible to actual gas flow ratio as:

$$V_b = (1-\beta)\,\kappa\,\frac{Q}{n_b} \tag{16}$$

where β indicates the amount of volatile matter that percolates through the emulsion phase, whereas κ takes into account the correction on the kinetic of devolatilization, which was assumed to follow a pseudo-first order rate law for ease of discussion. The volumetric flow rate of volatiles released by the particle can be expressed by the following equation [13–15,66]:

$$Q = \frac{m_{p0}\,w}{\rho_{vm}} k e^{-kt} \tag{17}$$

The density of volatile matter ρ_{vm} was calculated assuming phenol as ideal gaseous pseudo-component [23], which is equal to 1.14 kg/m^3 in the present case. Typical value of volatile content w for beech wood is 0.85 [56,57]. The reaction rate constant k is 0.0226 s^{-1} and was calculated by means of the Arrhenius-type equation with values of pre-exponential factor and activation energy of 0.0807 s^{-1} and 10.6 kJ/mol, respectively [22].

Since the residence time of the biomass particle within the bed is relatively low compared to the characteristic devolatilization time, exponential term approaches to unity (kt approaches to zero) and Eq. 17 becomes:

$$Q = \frac{m_{p0}\,w}{\rho_{vm}} k \tag{18}$$

The superficial velocity of volatiles released that percolate through the emulsion phase can be calculated as:

$$U_{vm} = \beta \frac{Q}{S_{p0}} \tag{19}$$

where S_{p0} is the maximum cross-sectional area of the biomass particle. Finally, it is possible to define the relative endogenous bubble velocity as follows:

$$\alpha^* = \frac{U_{br}\ \varepsilon_{mf}}{U_{vm}} \tag{20}$$

Table 3 shows the results obtained from measurements on X-ray images.

Table 3: Results obtained from X-ray measurements for the assessment of cloud phase properties.

Bubble (#)	$\mathbf{u_{br,exp}}$ **(cm/s)**	$\mathbf{u_{br,calc}}$ **(cm/s)**	**β**	**κ**	**γ**	$\mathbf{U_{vm}}$ **(cm/s)**	$\mathbf{\alpha^*}$	$\mathbf{r_c/r_b}$
1	23.2	36.3	0.547	14.7	6.67	5.70	1.92	1.33
2	26.5	36.8	0.665	21.0	7.04	6.93	1.81	1.30
3	23.2	39.4	0.684	32.6	10.3	7.12	1.54	1.18
4	53.0	36.9	0.165	8.35	6.96	1.72	14.5	1.30
5	30.9	40.3	0.514	24.3	11.79	5.36	2.73	1.18
6	36.4	29.7	0.341	3.66	2.41	3.55	4.85	1.32
7	34.2	30.4	0.299	3.90	2.73	3.11	5.19	1.33
8	27.6	33.5	0.344	6.56	4.30	3.58	3.64	1.26
9	25.9	32.5	0.600	8.00	3.20	6.25	1.96	1.72
10	39.3	31.7	0.438	5.62	3.16	4.56	4.08	1.88
11	47.7	39.9	0.170	8.30	6.88	1.77	12.7	1.05
12	29.7	30.0	0.580	4.20	1.76	6.04	2.33	1.89
13	34.7	35.9	0.710	21.5	6.23	7.39	2.22	1.47
14	30.2	30.7	0.0375	9.63	9.26	0.390	36.5	0.834
15	31.5	35.5	0.260	7.40	5.48	2.71	5.50	1.52
16	46.1	32.8	0.380	6.20	3.84	3.96	5.50	1.66
17	41.3	34.3	0.290	7.10	5.04	3.02	6.45	1.21
18	26.8	30.2	0.747	10.6	2.70	7.78	1.63	1.92

Values of α^* higher than unity in all the cases investigated confirm the presence of a cloud around the rising endogenous bubbles, in agreement with hydrodynamic theories [32]. It can be noted that the average value of beta is 0.432, meaning that about 43% of the gas released by the biomass particle percolates through the emulsion and the remaining 57% generates the endogenous bubble. It is interesting to note that this result is in good agreement with the behaviour observed for an isolated bubble in a bed at minimum fluidization, after being injected through an orifice. According to Nguyen and Leung, the leakage of gas into the emulsion phase for a bed of alumina particles accounted for 47% [67]. Rowe et al. found that the visible bubble flow was approximately 50% of the gas injected into the bed for different types of bed materials, using X-ray cinematography [68]. Furthermore, the parameter γ has an average value of 5.54, which follows the trend obtained in a previous study [22]. Table 3 also shows a comparison between experimental and calculated velocity for endogenous bubbles. The experimental velocity $u_{br,exp}$ was measured considering the distance covered by a bubble between two consecutive X-ray frames. For the calculation, the following well-known correlation was used [32]:

$$u_{br,calc} = 0.711\sqrt{g\ d_b} \tag{21}$$

It is interesting to note that there are inconsistencies between the measured and calculated values of velocity, as observed in Table 3. This appears to be in contrast with previous observations, that is endogenous and exogenous bubbles behave in a similar way. However, Rowe and Partridge investigated exogenous bubbles velocity for different bed materials and fitted their values assuming a generic coefficient for Eq. 21, as follows [50]:

$$u_{br} = \phi\sqrt{g\ d_b} \tag{22}$$

The authors obtained a great scattering for the coefficient Φ in Eq. 22, which varied in the range of 0.590 – 0.856 according to the particle size of the bed material. Therefore, they observed that there is no specific experimental reason for choosing this type of equation. Figure 8 shows the experimental values of rising bubble velocity obtained in this work, along with the best fitting curve (Eq. 22).

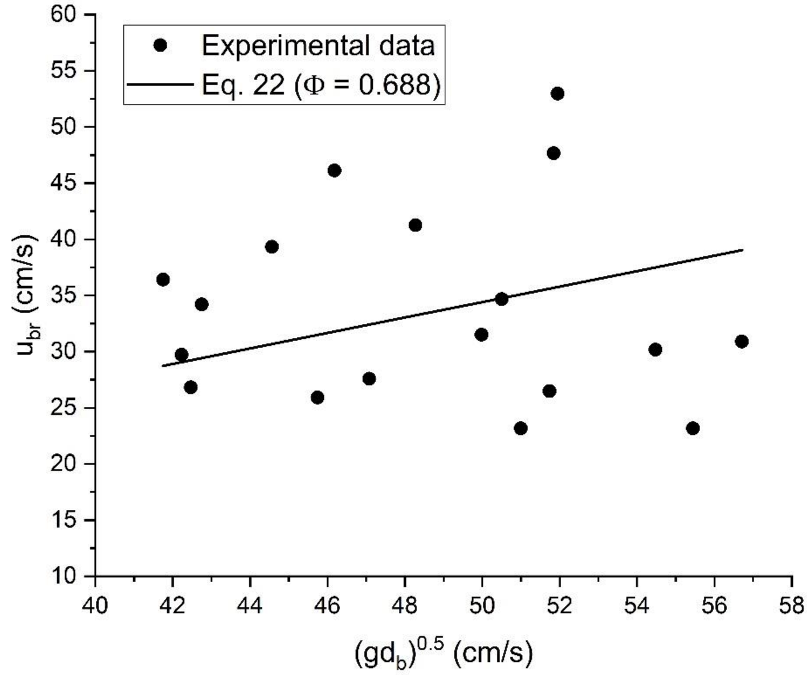

Figure 8: Experimental values of rising bubble's velocity as a function of the right-hand side of Eq. 22.

The coefficient obtained from the fitting procedure is 0.688 (R^2 = 0.93), which is similar to the value obtained by Rowe and Partridge. They found values of Φ in the range of 0.651 – 0.706 for bed materials with an average particle size between 220 and 240 µm, that is very close to the one used in this study (250 µm). It is then possible to conclude that the analogy between endogenous and exogenous bubbles is still verified.

Figure 9 shows theoretical and experimental r_c to r_b ratios as a function of α^*. The Murray's equation has been solved assuming different values of ω, due to the difficulty in determining this parameter from experiments.

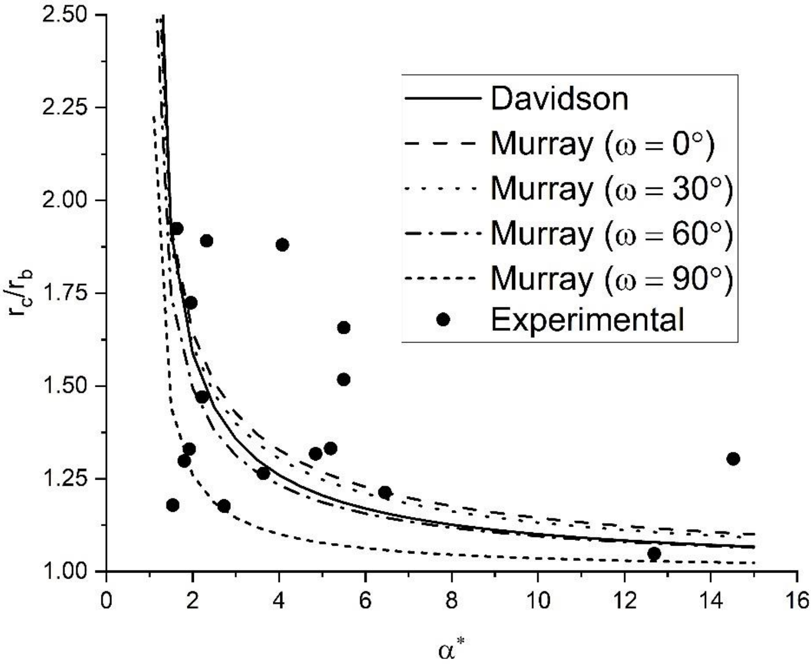

Figure 9: Ratio between cloud and bubble radius as a function of the relative endogenous bubble's velocity.

Most of the experimental values are uniformly distributed around the theoretical curves, suggesting an effective recirculation of volatile matter within the bubble to form the cloud region. However, there are few points scattered above the curves. In these cases, the observed endogenous bubbles developed a relatively large cloud region compared to the predicted one. This might indicate that these bubbles and their associated clouds had not reached the steady state required by the hydrodynamic theories, even if they were nearly at the surface of the bed. This result is in agreement with an X-ray investigation conducted by Rowe and Yacono, who found large differences between the visible bubble volumes and those expected by the two-phase theory [69]. Furthermore, it is important to note that the particle's devolatilization at the conditions studied follows a multiple bubble segregation pattern [14,15,22], which may result in the occurrence of coalescence of two or more bubbles before their eruption at the surface of the bed. This observation implies that the endogenous bubbles released were not necessarily fully developed before bursting at the surface of the bed, explaining the deviation from theoretical values.

4. Conclusions

This work focused on the investigation of structure and properties of endogenous bubbles released by a biomass particle during devolatilization at 730 °C. During each experimental run, a single 12-mm sphere of beech wood was injected from the bottom of the bed fluidized by nitrogen. The bed was operated at minimum fluidization condition, in order to visualize the endogenous bubbles without any disruption arising from exogenous bubbles. A non-intrusive X-ray imaging technique has been used for the investigation, showing good reliability and precision in defining the structure of the bubbles observed. Void fraction distribution obtained from the Beer-Lambert law was consistent with the expected values. Void fraction varied in a range of 0.47 to 0.78, corresponding to emulsion phase of the expanded bed at minimum fluidization and centre of the bubbles, respectively.

A comprehensive assessment of the bubble's shape has shown the presence of a wake, cloud and a region rich in gas, resembling the structure of an exogenous bubble. Values of wake fraction of 0.25 found in this study are in good agreement with results obtained from other researchers for natural sand as bed material. However, the mechanism of cloud formation is more complex and required a closer investigation. It was assumed that the volatiles percolating through the bed emulsion and traveling behind a rising bubble are the only responsible for the generation of the cloud region. Results confirmed the establishment of fast clouded bubbles regime, since the measured endogenous bubbles velocities were always higher than the velocity of the volatile matter percolating through the emulsion phase, in agreement with the Davidson's theory. However, the cloud to bubble size ratio was not always in agreement with the hydrodynamic theories. The differences observed have been attributed to the occurrence of coalescence between multiple endogenous bubbles after being released, which can cause delay in the development of the bubbles themselves before reaching the surface of the bed.

The results obtained in this work highlight the strong similarity between exogenous bubbles, whose structure has been extensively investigated in the past by several researchers, and endogenous bubbles released during devolatilization of a highly volatile solid feedstock. These findings have important implications for the modelling of continuous thermochemical operations in bubbling fluidized bed reactors, since the large amount of volatile matter released by biomass feedstock may have a significant effect on the hydrodynamic of the bed. However, further investigations need to be conducted to better understand how the coalescence phenomena between multiple endogenous bubbles (and endogenous and exogenous bubbles) can affect the mixing between volatiles and fluidizing gas within the bed and, ultimately, the performance of the entire thermochemical process.

Acknowledgment

The authors wish to acknowledge UK Research and Innovation (UKRI) for funding this research project. The authors also thank the UCL Bioenergy Technologies Research Lab and its members Alex Sebastiani, Matteo Errigo and Suviti Chari for sharing thoughts during the writing of this manuscript.

Nomenclature

Symbols	
c [-]	Concentration of bed solids
d [m]	Diameter
f_w [-]	Fraction of wake of endogenous bubble
I [-]	Transmitted intensity of the X-ray beam
I_0 [-]	Incident intensity of the X-ray beam
k [s^{-1}]	Reaction rate constant
L [m]	Path length of X-ray beam
m [kg]	Mass
Q [m^3/s]	Volumetric flow rate of volatiles
r [m]	Radius
S [m^2]	Maximum cross-sectional area
U [m/s]	Superficial velocity
V [m^3]	Volume
w [-]	Mass composition of volatile matter in feedstock
Greek letters	
α^* [-]	Relative endogenous bubble velocity

β [-]	Fraction of volatile matter percolating through the emulsion
γ [-]	Proportional constant in Eq. 15
ε [-]	Void fraction
θ_w [deg]	Wake angle
κ [-]	Kinetic parameter in Eq. 16
μ [m^{-1}]	Linear attenuation coefficient
ρ [kg/m^3]	Density
ϕ [-]	Coefficient in Eq. 22
ω [deg]	Physical parameter in Eq. 14
Subscripts	
0	Initial
b	Endogenous bubble
br	Rising endogenous bubble
c	Cloud region
mf	Minimum fluidization
p	Biomass particle
vm	Volatile matter
w	Wake region
Acronyms	
BW	Beech wood

References

[1] J. Fuchs, J.C. Schmid, S. Müller, H. Hofbauer, Dual fluidized bed gasification of biomass with selective carbon dioxide removal and limestone as bed material: A review, Renew. Sustain. Energy Rev. 107 (2019) 212–231. https://doi.org/10.1016/j.rser.2019.03.013.

[2] M.M. Jaffar, M.A. Nahil, P.T. Williams, Synthetic natural gas production from the three stage (i) pyrolysis (ii) catalytic steam reforming (iii) catalytic hydrogenation of waste biomass, Fuel Process. Technol. 208 (2020) 106515. https://doi.org/10.1016/j.fuproc.2020.106515.

[3] G. Amaya-Santos, S. Chari, A. Sebastiani, F. Grimaldi, P. Lettieri, M. Materazzi, Biohydrogen: A life cycle assessment and comparison with alternative low-carbon production routes in UK, J. Clean. Prod. 319 (2021) 128886. https://doi.org/10.1016/j.jclepro.2021.128886.

[4] M. Materazzi, P.U. Foscolo, The role of waste and renewable gas to decarbonize the energy sector, in: Substit. Nat. Gas from Waste, Elsevier, 2019: pp. 1–19.

https://doi.org/10.1016/B978-0-12-815554-7.00001-5.
[5] Q. He, Q. Guo, K. Umeki, L. Ding, F. Wang, G. Yu, Soot formation during biomass gasification: A critical review, Renew. Sustain. Energy Rev. 139 (2021) 110710. https://doi.org/10.1016/j.rser.2021.110710.
[6] S. Iannello, S. Morrin, M. Materazzi, Fluidised bed reactors for the thermochemical conversion of biomass and waste†, KONA Powder Part. J. 37 (2020) 114–131. https://doi.org/10.14356/kona.2020016.
[7] I. Mema, K.A. Buist, J.T. Padding, Fluidization of spherical versus elongated particles : Experimental investigation using magnetic particle tracking, (2020) 1–13. https://doi.org/10.1002/aic.16895.
[8] I. Mema, J.T. Padding, Spherical versus elongated particles – Numerical investigation of mixing characteristics in a gas fluidized bed, Chem. Eng. Sci. X. 8 (2020) 100079. https://doi.org/10.1016/j.cesx.2020.100079.
[9] Y. Bai, H. Si, Experimental study on fluidization, mixing and separation characteristics of binary mixtures of particles in a cold fluidized bed for biomass fast pyrolysis, Chem. Eng. Process. - Process Intensif. 153 (2020) 107936. https://doi.org/10.1016/j.cep.2020.107936.
[10] L.-J. Wang, G.-C. Wei, S.-P. Duan, Q.-F. Hou, CFD-DEM study on the mixing characteristics of binary particle systems in a fluidized bed of refuse-derived fuel, Part. Sci. Technol. 37 (2019) 51–59. https://doi.org/10.1080/02726351.2017.1338320.
[11] B. Szücs, P. Szentannai, Experimental Investigation on Mixing and Segregation Behavior of Oxygen Carrier and Biomass Particle in Fluidized Bed, Period. Polytech. Mech. Eng. 63 (2019) 188–194. https://doi.org/10.3311/PPme.13764.
[12] M. Urciuolo, R. Solimene, P. Ammendola, S. Krusch, V. Scherer, P. Salatino, R. Chirone, O. Senneca, On the agglomeration tendency of carbonaceous fuels in fluidized beds, Fuel. 277

(2020) 118187. https://doi.org/10.1016/j.fuel.2020.118187.

[13] G. Bruni, R. Solimene, A. Marzocchella, P. Salatino, J.G. Yates, P. Lettieri, M. Fiorentino, Self-segregation of high-volatile fuel particles during devolatilization in a fluidized bed reactor, Powder Technol. 128 (2002) 11–21. https://doi.org/10.1016/S0032-5910(02)00149-3.

[14] M. Fiorentino, A. Marzocchella, P. Salatino, Segregation of fuel particles and volatile matter during devolatilization in a fluidized bed reactor - II. Experimental, Chem. Eng. Sci. 52 (1997) 1909–1922. https://doi.org/10.1016/S0009-2509(97)00019-5.

[15] M. Fiorentino, A. Marzocchella, P. Salatino, Segregation of fuel particles and volatile matter during devolatilization in a fluidized bed reactor - I. Model development, Chem. Eng. Sci. 52 (1997) 1893–1908. https://doi.org/10.1016/S0009-2509(97)00018-3.

[16] P. Salatino, R. Solimene, Mixing and segregation in fluidized bed thermochemical conversion of biomass, Powder Technol. 316 (2017) 29–40. https://doi.org/10.1016/j.powtec.2016.11.058.

[17] K.S. Jaya Bharathi. J., Hydrodynamics and Particle Mixing Characteristics of a Ternary Mixture in a Gas-Solid Fluidized Bed, Int. J. Recent Technol. Eng. 8 (2019) 2520–2526. https://doi.org/10.35940/ijrte.D7120.118419.

[18] M.S. Alagha, B. Szucs, P. Szentannai, Numerical study of mixing and heat transfer of SRF particles in a bubbling fluidized bed, J. Therm. Anal. Calorim. 142 (2020) 1087–1096. https://doi.org/10.1007/s10973-019-09135-2.

[19] M. Fiorentino, A. Marzocchella, P. Salatino, Segregation of fuel particles and volatile matter during devolatilization in a fluidized bed reactor—II. Experimental, Chem. Eng. Sci. 52 (1997) 1909–1922. https://doi.org/10.1016/S0009-2509(97)00019-5.

[20] A.C. Rees, J.F. Davidson, J.S. Dennis, A.N. Hayhurst, The rise of buoyant fuel-particles in a slugging gas-fluidized combustor, Chem. Eng. Res. Des. 84 (2006) 319–327.

https://doi.org/10.1205/cherd05043.

[21] R. Solimene, A. Marzocchella, P. Salatino, Hydrodynamic interaction between a coarse gas-emitting particle and a gas fluidized bed of finer solids, Powder Technol. 133 (2003) 79–90. https://doi.org/10.1016/S0032-5910(03)00080-9.

[22] S. Iannello, P.U. Foscolo, M. Materazzi, Investigation of single particle devolatilization in fluidized bed reactors by X-ray imaging techniques, Chem. Eng. J. 431 (2022) 133807. https://doi.org/10.1016/j.cej.2021.133807.

[23] A. Gómez-Barea, B. Leckner, Modeling of biomass gasification in fluidized bed, Prog. Energy Combust. Sci. 36 (2010) 444–509. https://doi.org/10.1016/j.pecs.2009.12.002.

[24] M.B. Nikoo, N. Mahinpey, Simulation of biomass gasification in fluidized bed reactor using ASPEN PLUS, 32 (2008) 1245–1254. https://doi.org/10.1016/j.biombioe.2008.02.020.

[25] D. Fiaschi, M. Michelini, A two-phase one-dimensional biomass gasification kinetics model, Biomass and Bioenergy. 21 (2001) 121–132. https://doi.org/10.1016/S0961-9534(01)00018-6.

[26] J. Corella, A. Sanz, Modeling circulating fluidized bed biomass gasifiers . A pseudo-rigorous model for stationary state, 86 (2005) 1021–1053. https://doi.org/10.1016/j.fuproc.2004.11.013.

[27] J. Corella, J.M. Toledo, G. Molina, Calculation of the conditions to get less than 2 g tar / m n in a fluidized bed biomass gasifier, 87 (2006) 841–846. https://doi.org/10.1016/j.fuproc.2006.05.002.

[28] I. Petersen, J. Werther, Experimental investigation and modeling of gasification of sewage sludge in the circulating fluidized bed, 44 (2020) 717–736. https://doi.org/10.1016/j.cep.2004.09.001.

[29] L. Yu, J. Lu, X. Zhang, Numerical simulation of the bubbling fluidized bed coal gasification by

the kinetic theory of granular flow (KTGF), 86 (2007) 722–734. https://doi.org/10.1016/j.fuel.2006.09.008.

[30] A. Sebastiani, D. Macrì, K. Gallucci, M. Materazzi, Steam - oxygen gasification of refuse derived fuel in fluidized beds: Modelling and pilot plant testing, Fuel Process. Technol. 216 (2021) 106783. https://doi.org/10.1016/j.fuproc.2021.106783.

[31] A. Di Carlo, D. Borello, E. Bocci, G. Marconi, V. Virgilio, Process simulation of a hybrid SOFC/mGT and enriched air/steam fluidized bed gasifier power plant, Int. J. Hydrogen Energy. 38 (2013) 5857–5874. https://doi.org/10.1016/j.ijhydene.2013.03.005.

[32] D. Kunii, O. Levenspiel, Fluidization Engineering (Second Edition), Fluid. Eng. 1 (1991) 1–13. https://doi.org/10.1016/B978-0-08-050664-7.50007-X.

[33] E.R. Gilliland, Fluidised particles, J. F. Davidson and D. Harrison, Cambridge University Press, New York(1963). 155 pages.$6.50, AIChE J. 10 (1964) 783–785. https://doi.org/10.1002/aic.690100503.

[34] P.N. Rowe, B.A. Partridge, Cloud formation around bubbles in gas fluidized beds, 19 (1964) 973–985.

[35] T. Wytrwat, M. Yazdanpanah, S. Heinrich, Bubble Properties in Bubbling and Turbulent Fluidized Beds for Particles of Geldart ’ s Group B, (2020).

[36] R. Jackson, Instabilities and the formation of bubbles in fluidized beds, (1995) 327–366.

[37] P.N. Rowe, A.W. Nienow, Particle mixing and segregation in gas fluidised beds. A review, Powder Technol. 15 (1976) 141–147. https://doi.org/10.1016/0032-5910(76)80042-3.

[38] A. Soria-Verdugo, L.M. Garcia-Gutierrez, S. Sanchez-Delgado, U. Ruiz-Rivas, Circulation of an object immersed in a bubbling fluidized bed, Chem. Eng. Sci. 66 (2011) 78–87. https://doi.org/10.1016/j.ces.2010.10.006.

[39] A. Soria-Verdugo, L.M. Garcia-Gutierrez, N. García-Hernando, U. Ruiz-Rivas, Buoyancy effects

on objects moving in a bubbling fluidized bed, Chem. Eng. Sci. 66 (2011) 2833–2841. https://doi.org/10.1016/j.ces.2011.03.055.

[40] B. Cluet, G. Mauviel, Y. Rogaume, O. Authier, A. Delebarre, Segregation of wood particles in a bubbling fluidized bed, Fuel Process. Technol. 133 (2015) 80–88. https://doi.org/10.1016/j.fuproc.2014.12.045.

[41] M. Stein, Y.L. Ding, J.P.K. Seville, D.J. Parker, Solids motion in bubbling gas fluidized beds, Chem. Eng. Sci. 55 (2000) 5291–5300. https://doi.org/10.1016/S0009-2509(00)00177-9.

[42] Y.S. Wong, J.P.K. Seville, Single-Particle Motion and Heat Transfer in Fluidized Beds, 52 (2006) 4099–4109. https://doi.org/10.1002/aic.

[43] F. Fotovat, J. Chaouki, Characterization of the upward motion of an object immersed in a bubbling fluidized bed of fine particles, Chem. Eng. J. 280 (2015) 26–35. https://doi.org/10.1016/j.cej.2015.05.130.

[44] F. Fotovat, R. Ansart, M. Hemati, O. Simonin, J. Chaouki, Sand-assisted fluidization of large cylindrical and spherical biomass particles: Experiments and simulation, Chem. Eng. Sci. 126 (2015) 543–559. https://doi.org/10.1016/j.ces.2014.12.022.

[45] A. Köhler, D. Pallarès, F. Johnsson, Modeling Axial Mixing of Fuel Particles in the Dense Region of a Fluidized Bed, Energy and Fuels. (2020). https://doi.org/10.1021/acs.energyfuels.9b04194.

[46] A. Köhler, A. Rasch, D. Pallarès, F. Johnsson, Experimental characterization of axial fuel mixing in fluidized beds by magnetic particle tracking, Powder Technol. 316 (2017) 492–499. https://doi.org/10.1016/j.powtec.2016.12.093.

[47] A. Köhler, D. Pallarès, F. Johnsson, Magnetic tracking of a fuel particle in a fluid-dynamically down-scaled fluidised bed, Fuel Process. Technol. 162 (2017) 147–156. https://doi.org/10.1016/j.fuproc.2017.03.018.

[48] W. Yoshimori, T. Ikegai, K. Uemoto, S. Narita, S. Harada, J. Oshitani, Non - invasive measurement of floating – sinking motion of a large object in a gas – solid fluidized bed, Granul. Matter. 21 (2019) 1–11. https://doi.org/10.1007/s10035-019-0897-3.

[49] F. Hossein, M. Materazzi, P. Lettieri, P. Angeli, Application of acoustic techniques to fluid-particle systems – A review, Chem. Eng. Res. Des. 176 (2021) 180–193. https://doi.org/10.1016/j.cherd.2021.09.031.

[50] P.N. Rowe, B.A. Partridge, An x-ray study of bubbles in fluidised beds, Chem. Eng. Res. Des. 75 (1965) S116–S134. https://doi.org/10.1016/S0263-8762(97)80009-3.

[51] J.G. Yates, D.J. Cheesman, B. Engineering, Experimental Observations of Voidage Distribution, Chem. Eng. Sci. 49 (1994) 1885–1895.

[52] L. Panariello, M. Materazzi, R. Solimene, P. Salatino, P. Lettieri, X-ray imaging of horizontal jets in gas fluidised bed nozzles, Chem. Eng. Sci. 164 (2017) 53–62. https://doi.org/10.1016/j.ces.2017.01.055.

[53] L. Panariello, D. Macrí, V. Zito, R. Solimene, P. Salatino, P. Lettieri, M. Materazzi, Experimental and numerical analysis of jet penetration and gas evolution in a single-nozzle distributor fluidized bed, Chem. Eng. J. 437 (2022) 135391. https://doi.org/10.1016/j.cej.2022.135391.

[54] F. Scala, Fluidized Bed Technologies for Near-Zero Emission Combustion and Gasification, 2013. https://doi.org/10.1533/9780857098801.frontmatter.

[55] H.L. Zhu, Y.S. Zhang, M. Materazzi, G. Aranda, D.J.L. Brett, P.R. Shearing, G. Manos, Co-gasification of beech-wood and polyethylene in a fluidized-bed reactor, Fuel Process. Technol. 190 (2019) 29–37. https://doi.org/10.1016/j.fuproc.2019.03.010.

[56] M. Rabacal, M. Costa, M. Vascellari, C. Hasse, Kinetic modelling of sawdust and beech wood pyrolysis in drop tube reactors using advanced predictive models, Chem. Eng. Trans. 37 (2014) 79–84. https://doi.org/10.3303/CET1437014.

[57] C. Guizani, M. Jeguirim, S. Valin, L. Limousy, S. Salvador, Biomass chars: The effects of pyrolysis conditions on their morphology, structure, chemical properties and reactivity, Energies. 10 (2017). https://doi.org/10.3390/en10060796.

[58] D. Macrì, S. Sutcliffe, P. Lettieri, Fluidized bed sintering in TiO2 and coke systems, Chem. Eng. J. 381 (2020) 122711. https://doi.org/10.1016/j.cej.2019.122711.

[59] D. Macrì, M. Poletto, D. Barletta, P. Lettieri, An investigation of the fl ow properties of rutile particles : Fluidization behaviour linked with shearing studies, 374 (2020) 544–559. https://doi.org/10.1016/j.powtec.2020.07.082.

[60] J.G. Yates, D.J. Cheesman, P. Lettieri, D. Newton, X-ray analysis of fluidized beds and other multiphase systems, KONA Powder Part. J. 20 (2002) 133–143. https://doi.org/10.14356/kona.2002016.

[61] J.G. Yates, S.J.R. Simons, Experimental methods in fluidization research, Int. J. Multiph. Flow. 20 (1994) 297–330. https://doi.org/10.1016/0301-9322(94)90076-0.

[62] S. Tebianian, N. Ellis, P. Lettieri, J.R. Grace, X-ray imaging for flow characterization and investigation of invasive probe interference in travelling fluidized bed, Chem. Eng. Res. Des. 104 (2015) 191–202. https://doi.org/10.1016/j.cherd.2015.08.006.

[63] Y. Lu, J. Huang, P. Zheng, D. Jing, Flow structure and bubble dynamics in supercritical water fluidized bed and gas fluidized bed : A comparative study, Int. J. Multiph. FLOW. 73 (2015) 130–141. https://doi.org/10.1016/j.ijmultiphaseflow.2015.03.011.

[64] F. Fotovat, J. Chaouki, J. Bergthorson, The effect of biomass particles on the gas distribution and dilute phase characteristics of sand-biomass mixtures fluidized in the bubbling regime, Chem. Eng. Sci. 102 (2013) 129–138. https://doi.org/10.1016/j.ces.2013.07.042.

[65] E. Cano-pleite, A. Soria-verdugo, D. Pallar, Modeling the motion of fuel particles in a fluidized bed, 305 (2021). https://doi.org/10.1016/j.fuel.2021.121424.

[66] N. Jand, P.U. Foscolo, Decomposition of wood particles in fluidized beds, Ind. Eng. Chem. Res. 44 (2005) 5079–5089. https://doi.org/10.1021/ie040170a.

[67] X.T. Nguyen, L.S. Leung, A note on bubble Formation at an orifice in a fluidised bed, Chem. Eng. Sci. 27 (1972) 433–434. https://doi.org/10.1038/190433a0.

[68] J.A.M. Kuipers, W. Prins, W.P.M. van Swaaij, Theoretical and Experimental Bubble Formation at a Single Orifice in a Two-dimensional Gas-fluidized Bed, Chem. Eng. Sci. 46 (1991) 2881–2894.

[69] P.N. Rowe, C.X.R. Yacono, The Bubbling Behaviour of Fine Powders when Fluidised, 31 (1976) 1179–1192.